WILEY-VCH

Enhancing Cycling Stability and Capacity Retention of NMC811 Cathodes by Reengineering Interfaces via Electrochemical Fluorination

Bishnu P. Thapaliya, Sudhajit Misra, Shi-ze Yang, Charl J. Jafta, Harry M. Meyer III, Prashant Bagri, Raymond R. Unocic, Craig A. Bridges, Sheng Dai**

Dr. Bishnu P. Thapaliya, Dr. Harry M. Meyer III, Dr. Prashant Bagri, Dr. Craig A. Bridges, Prof. Sheng Dai
Chemical Sciences Division, Oak Ridge National Laboratory, Oak Ridge, TN 37831, USA
E-mail: prasadthapab@ornl.gov, dais@ornl.gov,

Dr. Bishnu P. Thapaliya, Prof. Sheng Dai
Department of Chemistry, Joint Institute for Advanced Materials, University of Tennessee, Knoxville, TN 37996, USA

Dr. Sudhajit Misra, Dr. Raymond R. Unocic
Center for Nanophase Materials Sciences, Oak Ridge National Laboratory, Oak Ridge, TN 37831, USA

Dr. Charl J. Jafta
Electrification and Energy Infrastructure Division, Oak Ridge National Laboratory, Oak Ridge, TN 37830, USA

Dr. Shi-ze Yang
Eyring Materials Center, Arizona State University, Tempe, Arizona 85287

Keywords: Electrochemical fluorination (ECF), high-capacity cathodes, conformal LiF, high energy density battery, electromaterial functionalization

Abstract

High-capacity cathodes ($LiNi_{0.8}Mn_{0.1}Co_{0.1}O_2$) that can boost the energy density of lithium-ion batteries (LIBs) are promising candidates for vehicle electrification. However, several factors specific to high energy density materials entailing electrode reactions inhibit their application. Fluorination has shown a promising ability to combat the detrimental electrochemical performances of cathode materials, however, it remains difficult to achieve the desired functionality. Herein, we propose a novel electrochemical fluorination (ECF) that demonstrates a promising electrochemical performance enhancement via stabilization of the cathode-electrolyte-interphase (CEI) by forming conformal LiF. Besides LiF surface layer formation, ECF reduces the degree of fluorination-induced Ni/Li disordering and enhances the layered structural stability as probed by X-ray diffraction (XRD). Because of the robust CEI, ECF-NMC811 cathodes delivered 203.0 mAh g^{-1} first discharge capacity at the current rate of C/10, with ~ 98 % capacity retention up to 100 cycles. Similarly, it delivers ~180 mAh g^{-1} capacity at a 1C rate with 86.4 % capacity retention up to 200 cycles with average coulombic efficiency of > 99.5 %. Comprehensive characterization with a multitude of probes reveals that ECF enhances the cycling stability of the electrode without altering bulk structure and morphology.

1. Introduction

Among the various storage systems available, lithium-ion batteries (LIBs) dominate the current market for energy storage devices.[1-3] Currently, graphite is used as the anode in commercial LIBs with a specific theoretical gravimetric capacity of 372 mAh g^{-1}. The conventional cathode materials are $LiCoO_2$, $LiFePO_4$, and $LiMn_xNi_{1-x-y}CoyO_2$ (NMC), with specific capacities ranging from 140 mAh g^{-1} to 200 mAh g^{-1}, which is the capacity limiting electrode that determines the energy density of a cell. Therefore, it is essential to develop high-energy-density cathode materials with long cycling stability and high capacity retention for the longer driving ranges that promote vehicle electrification.

To revolutionize electromobility, extensive research is being carried out on the high-capacity cathodes, amongst other cell components, with new approaches identified to optimize their performances.[4-6] $LiNi_{0.8}Mn_{0.1}Co_{0.1}O_2$ (NMC811 (80 % Ni)) is one of the most promising cathode materials and has been touted as the next generation high capacity cathode for vehicle electrification because of its low Co content and simultaneous high practical energy density (specific capacity of ~200 mAh g^{-1} and high discharge potential of ~3.8 V vs. Li/Li^+)[7-9], rate capability, and relatively lower cost. However, these high-energy cathodes with higher Ni content have suffered from structural instability, rapid capacity fading, and voltage evolution upon cycling. The instability of high voltage, high capacity cathodes originates from the reversible/irreversible phase transitions, particle cracking, oxygen evolution, transition metal cation dissolution, and detrimental side reactions with electrolytes at the electrode-electrolyte interphase leading to thick cathode electrolyte interphase (CEI).[10-15] Similarly, the rapid capacity fading of NMC811, when cycled above 70 % state of charge (SOC, >4.2 V), occurs due to reactive interfaces, electrolyte oxidation, parasitic side reaction, and surface phase transition to resistive rock salt structure leading to uncontrolled CEI growth[16], dissolution of transition metal cations, and collapsing of interlayer spacing and unit cell volume.[7] A variety of electrolytes have been studied and offer promising results, including highly fluorinated electrolytes, high-concentration electrolytes, and ether-based localized high-concentrated electrolytes with fluorine-containing salt and solvents.[17-22] In another approach to improve the structural stability, capacity retention, and minimize lattice doping with cations and anions, a buffer zone has been created by coating with oxide like TiO_2, ZrO_2, Al_2O_3 to avoid the surface reaction.[10, 23-25] However, these efforts are typically not practical for commercial applications for multiple reasons. It is a well-established fact that the battery can perform well, delivering enhanced capacity and cycling stability beyond the thermodynamic limit of the electrolyte, only when the cathode-electrolyte interphase is protected by a smooth passivating layer (e.g., LiF) that blocks the leaking of the electron from cathode to electrolyte while permitting ion transport.

The formation of a sub-nanolayer of LiF without altering bulk structure and morphology is challenging, and uncontrolled fluorination is detrimental to the cycling stability of the cathodes. However, among suitable passivation films for high capacity cathodes, a surface nanolayer of LiF is highly efficient as it is electrically insulating while permitting ion conduction that stabilizes the interphase.

Typically there are two main avenues for doping fluorine on the cathode surface, which are through (i) high temperature fluorination - a solid-state synthesis route[26, 27] or direct fluorination route by using F_2 gas as used by Dai et al. for transition metal oxides (TMOs)[28-35], or (ii) solution mediated fluorination – the use of fluorinated solvents or additives. Due to the advantages of fluorine chemistry at the interfaces during battery operation (i.e., forming a robust SEI[6], assisting in the retention of oxygen in the crystal lattice[36], enhancement of capacity, and cycling stability[15, 36, 37]), fluorination of cathodes have drawn significant interest as a unique technique for material functionalization. The existing fluorination methods are plagued by serious drawbacks, such as challenges in controlling sample morphology because of high energy process, expensive fluorinating agents (i.e., XeF_2), and the toxicity of using elemental F_2 gas. It is critical to develop control over the fluoride content in the surface film because excessive fluorination may lead to capacity and stability loss via the formation of O-TM-F bonds (TM=Ni, Co, Mn) that increases the impedance. [38, 39] Researchers are exploring effieient interfacial fluorination for energy storage materials to improve their performance by selectively tuning the thickness of the fluoride containing interphase.

Herein, for the first time, we demonstrate the formation of a robust, ionically conducting and electronically insulating LiF layer on the surface of NMC811 via ECF that exhibited enhanced cycling stability and capacity. The details of the experimental procedure and setup were presented in the experimental section and in the supporting information. This novel ECF method is shown to have many advantages over conventional fluorination methods, including minimal safety hazards, fast reaction kinetics, and easily controllable parameters (e.g., current,

voltage, time, and temperature, concentration of fluoride species) that result in an amorphous LiF surface layer on electrodes in lithium-ion containing electrolytes. Comprehensive characterization of surface and bulk structure and composition (XRD, X-ray photoelectron spectroscopy (XPS), high-resulution transmission electron microscopy (HR-TEM), scanning transmission electron microscopy-energy dispersive spectroscopy (STEM-EDS)) unravel the formation of conformal LiF layer that forms part of a robust CEI and shut down unwanted interfacial reactions, stabilizes the interphase, and enhances the cycling stability of the electrode without altering the bulk structure and morphology. Because of robust CEI stabilized by conformal LiF, the ECF-NMC811 cathode delivered 203.0 mAh g^{-1} discharge capacity at the current rate of C/10, ~200 mAh g^{-1} stable capacity up to 100 cycles with 98.0 % capacity retention at C/10 rate. Similarly, it delivers ~180 mAh g^{-1} capacity at a 1C rate with 86.4 % capacity retention up to 200 cycles with average coulombic efficiency of greater than 99.5 %. These promising results demonstrate the success of the novel ECF method, which could enable the practical application of NMC811 for vehicle electrification.

2. Results and Discussion

In order to study the possible structural changes imposed on the NMC811 samples due to ECF, XRD measurements were conducted on the respective pristine and fluorinated NMC811, as shown in **Figure 1**. The XRD patterns indicates that both pristine NMC811 and ECF-NMC811 (stored in ambient atmosphere) are single-phase layered rhombohedral $Li(NiCoMn)O_2$ with R-3M space group (JCPDS reference number: 01-080-7011). However, the XRD pattern of pristine NMC811 suggests that there is significant cation mixing and Ni/Li disordering. This is indicated by the ratio of the integrated intensity for the (003) and (104) reflections, I_{003}/I_{104} = 0.67, which is smaller than the theoretical ratio of 1.2; furthermore, we note the lack of splitting of the (006/012) reflections and broad splitting of the (018/110) reflections.[40-42] After ECF, I_{003}/I_{104} increases to 0.98, and the XRD pattern reveals sharp

splitting of (006/012) and (018/110) peaks that indicate the reduced Ni/Li disordering, which may be the reason for the better electrochemical performance for ECF-NMC811 than pristine NMC811 stored in ambient atmosphere, as described later.[23] Regardless of the initial structural NMC811, ECF tend to reduce Ni/Li disordering. To validate the cation ordering (Ni/Li) effect of ECF, ECF was carried out in fresh NMC811. The XRD pattern of the fresh NMC811 show sharp splitting of (006/012) and (018/110) peak with integrated I_{003}/I_{104} = 1.21, expected as a layered structure (**Figure S1**).

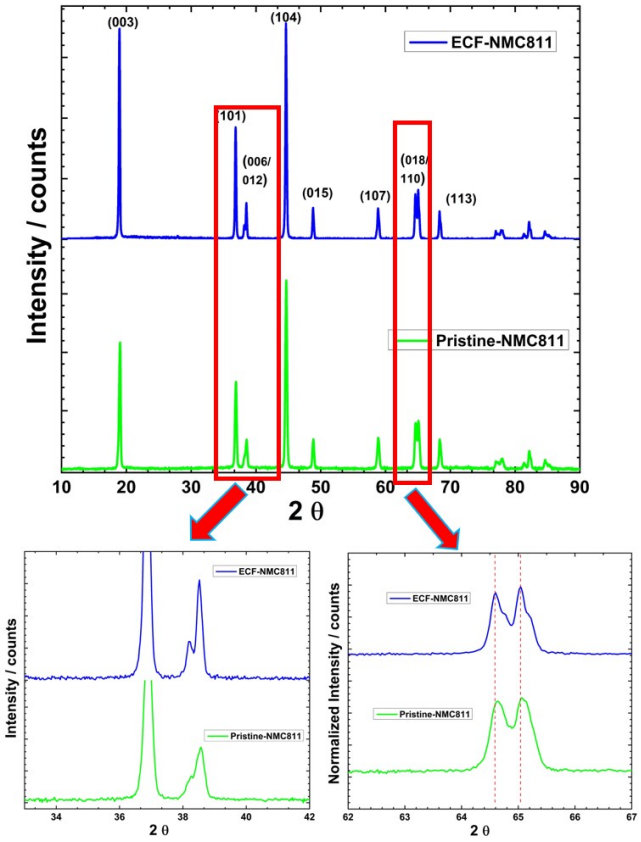

Figure 1. The XRD patterns of the pristine NMC811 store in ambient air for long time and ECF-NMC811 (Top: full XRD diffractogram, bottom-left: extend diffractogram showing the splitting peak at around 38.5°, and bottom-right: extended diffractogram showing the splitting peak around 65°.

After ECF, splitting of (006/012) and (018/110) peak become more pronounced with increasing Ni/Li ordering indicated by an increase in the value of integrated I_{003}/I_{104} = 1.38. The data were refined in R-3m with constraints on the 3b (0,0,1/2) and 3a (0,0,0) sites to full occupancy, and

with restraints on the chemical composition to near stoichiometric composition for Li and Ni. The Rietveld refinement results also suggest that ECF modification tends to reduce the amount of Ni/Li disordering; while the difference in ordering is small, the refinements suggest less Ni on the Li site (3b) in ECF samples and no Li on the Ni site (3a) in both samples, within error (see supplementary information for the details of Rietveld refinement results-**Table S1, S2, and Figure S2**). This observation suggests that ECF favors the reduction of Ni/Li disordering, and cation mixing that maintains the interlayer spacing intact and amount of active Ni and Li which favors enhanced Li-ion migration and electrochemical performance.[40, 41] Apart from this, XRD patterns do not show any detectable fluoride (e.g., any transition metal fluoride) which suggests either the formation of an amorphous or a very thin crystalline LiF surface layer which is under the detection limit of laboratory XRD.

Figure 2(a &b) shows the HR-STEM-ADF images of pristine NMC811 and ECF-NMC811 along (100) zone axis. The careful analysis of diffraction patterns (FFT) shows no change in atomic structure post ECF process and they exhibit the same lattice fringes correspond to a single phase rhombohedral layered oxide with the R-3M space group. The distribution of the different elements in the sample has been characterized by STEM -EDS, as shown in **Figure 2(c-h)** for ECF-NMC811. For ECF-NMC811, based on **Figure 2 (c-h), S3**, and **S4**, all the elements present (Ni, Co, Mn, O, and F) are distributed homogeneously with surface enrichment of the fluoride in ECF-NMC811. Therefore, STEM-EDS elemental mapping results suggest that electrochemical fluorination is an efficient fluorination method for tuning the fluorine content on the surface without altering the bulk structure and morphology.

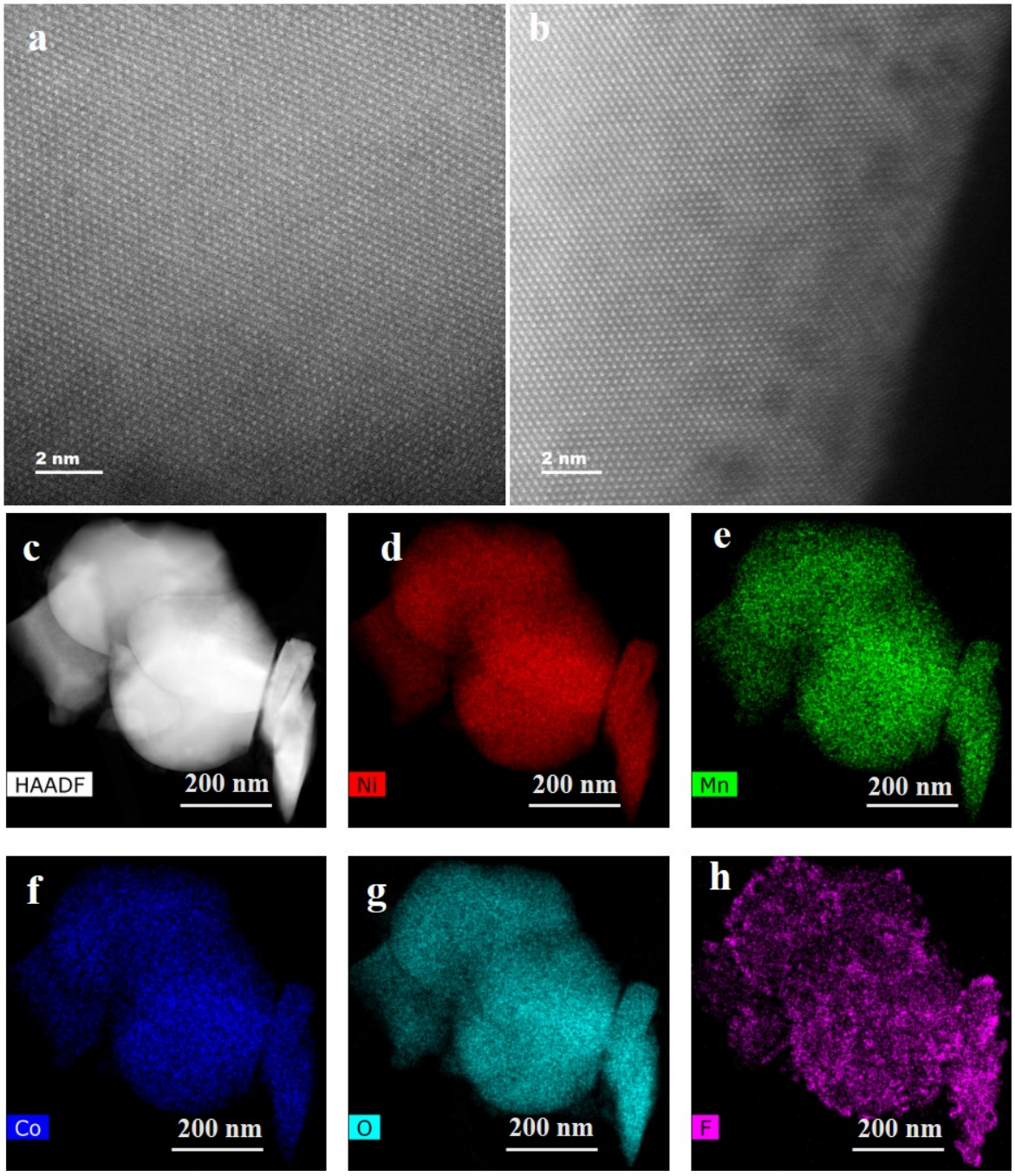

Figure 2. STEM-ADF images of (a) NCM 811 and (b) ECF-NMC811 along [100] zone axis showing no change in the atomic structure after the electrochemical fluorination process; STEM-EDS elemental mapping of an ECF-NMC811: (c) ADF image; image and the distribution of (d) Ni, (e) Mn, (f) Co, (g) O, and (h) F.

To study what surface species form with the use of the ECF on NMC811 particles, XPS was employed. **Figure 3** shows the XPS spectra of the F1s and O1s spectra for pristine and ECF-NMC811. The C-C binding energy (BE) peak at 284.8 eV is used for charge correction

for all the peaks for NMC811 samples. As expected, there are no F peaks observed for the pristine NMC811, as shown in **Figure 3a**.

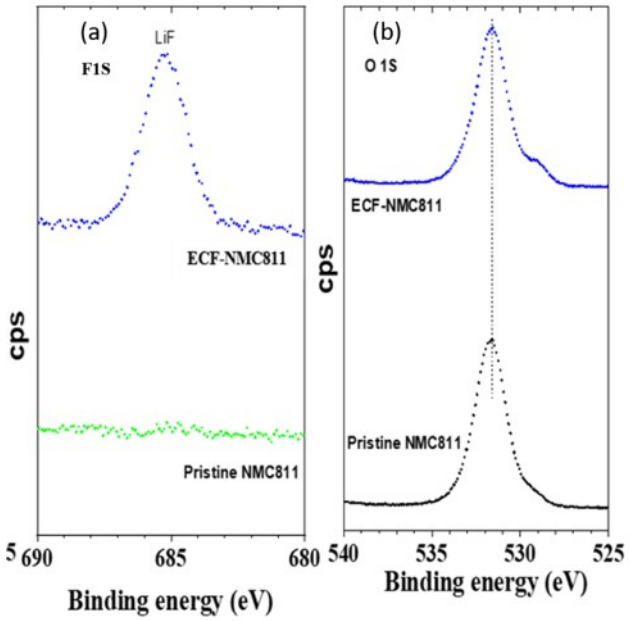

Figure 3. The pristine and ECF-NMC811 XPS of (a) the F1s and (b) O1s spectra.

For the ECF-NMC811, only one F peak is observed at a BE of 685.3 eV, which is indicative of the LiF surface layer. Surface LiF on an electrode is advantageous for forming a stable CEI that would stabilize the cathode-electrolyte interface resulting in stable battery cycling[6], avoiding the oxygen release, transition metal cations dissolution, and cracking down the detrimental cathode-electrolyte interfacial reaction. There is also no change observed in the metal oxidation states, as indicated by the lack of change in O 1s (**Figure 3b**) and the metal (Ni, Co, Mn) binding energies and peak positions (**Figure S5**), before and after ECF, indicating that there is no bulk fluorination (i.e., no transition metal fluoride).

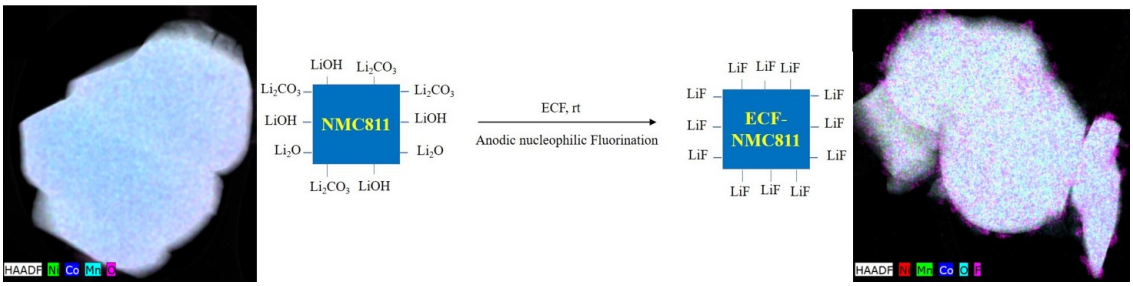

Scheme 1. Schematic representation of electrochemical fluorination showing the conversion of basic surface film to LiF enriched surface layer via anodic nucleophilic fluorination with STEM-EDS mapping of NMC811 and ECF-NMC811.

The results from comprehensive analysis techniques, including XRD, STEM-EDS, XPS, indicate that NMC811 was successfully fluorinated with surface enriched amorphous LiF layer. Nucleophilic fluorination induced by anodic polarization results in converting the basic surface film (LiOH, Li_2O, Li_2CO_3) of NMC811 into an ionically conducting thin amorphous LiF layer (Scheme 1) without altering the bulk structure. STEM-EDS and XPS data as well as cyclic voltammetry and charge discharge profiles (described later) validate the formation of LiF surface layer. Based on the experimental results and very high discharge potential of fluoride ion (>+2.9 V vs. SCE), the anodic nucleophilic fluorination may proceed via the formation of radical cation followed by nucleophilic attack by fluoride ion leading to the removal of oxygen atom(s) and resulting in the LiF surface layer (see mechanism and reaction scheme 2). This is in accordance with the mechanism reported in the literature for the ECF of organic compounds.[43] NMC811 is successfully fluorinated, forming LiF surface layers with relatively short reaction time and lower temperature than existing literature.[36] The bulk fluorination was avoided by applying mild ECF conditions (voltage, temperature, and shorter fluorination time) that limits the fluoride diffusion to the surface level. This novel method could be applied to fluorinate various inorganic solid materials for energy storage applications.

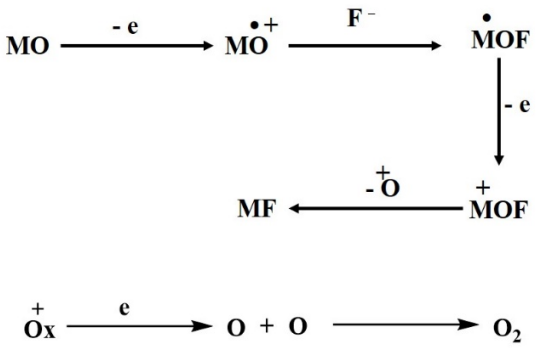

$$LiOH + 2F^{-} \rightarrow LiF + HF + {}^{1}/_{2}\, O_2 \qquad (1)$$

$$Li_2O + 2F^{-} \rightarrow 2LiF + {}^{1}/_{2}\, O_2 \qquad (2)$$

$$Li_2CO_3 + 2F^{-} \rightarrow 2LiF + CO_2 + {}^{1}/_{2}\, O_2 \qquad (3)$$

Scheme 2. Anodic electrode fluorination mechanism and possible surface reactions (1-3) for various lithium inorganic species on the surface of NMC811 during electrochemical fluorination.

The effectiveness of the surface LiF layer in stabilizing the electrochemical performance of NMC811 has been investigated in half cell configuration using lithium as a reference/counter electrode. Significant enhancement in the electrochemical performance for NMC811 cathode is observed post-fluorination. The cyclic voltammetry (CV) plot (**Figure 4a**) suggests a different nature for the first oxidation peak between NMC811 and ECF-NMC811. The high surface reactivity due to high Ni content leads to the formation of lithium carbonates/hydroxides on the electrode surfaces. Along with these insulating surface impurities, high reactivity leads to interfacial parasitic side reactions with electrolyte, which results in a first oxidation peak at the very high potential in the CV plot of NMC811. The formation of the LiF surface layer (observed in EDS mapping and verified by XPS) via ECF enhanced the ambient stability of

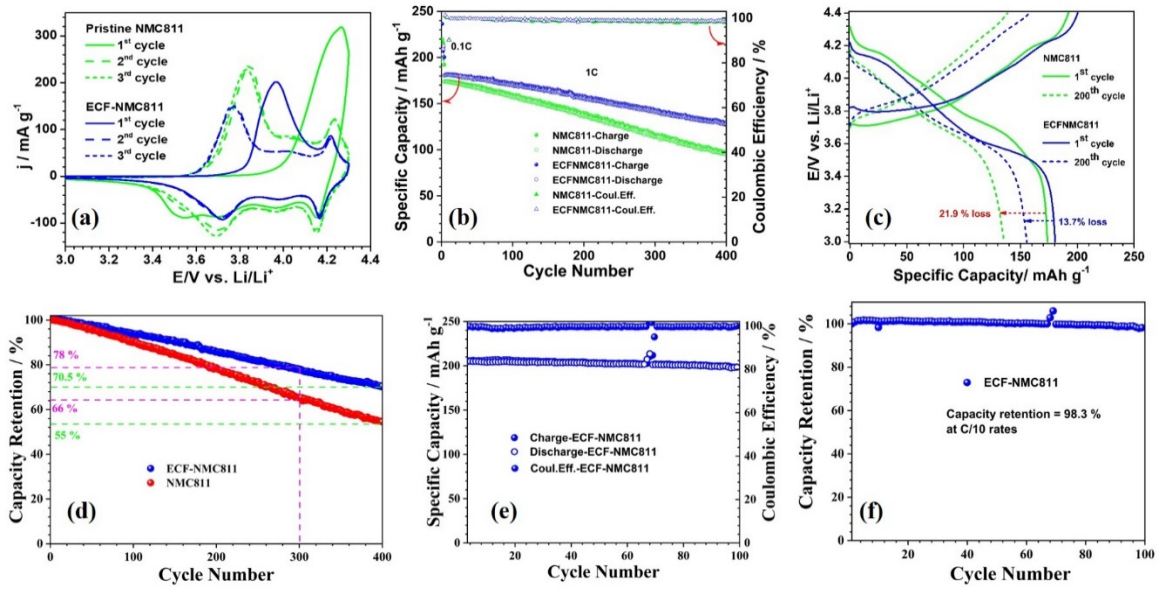

Figure 4. (a) Cyclic voltammograms of pristine NMC811 and ECF-NMC811 in the voltage range of 3.0- 4.3 V vs. Li/Li$^+$ at a 0.1 mV s^{-1} scan rate; (b) Discharge capacity and coulombic efficiency of pristine NMC811 and ECF-NMC811 from 3.0 – 4.4 V at 0.1 C for first two cycles and at 1C for long cycling; (c) respective charge-discharge profiles of pristine NMC811 and ECF-NMC811 from 3.0 – 4.4 V at 1C; (d) Showing capacity retention as a function of cycle number for pristine NMC811 and ECF-NMC811 from 4b; (e) Charge-discharge capacities and coulombic efficiency of ECF-NMC811 from 3.0 – 4.4 V at 0.1 C for 100 cycles and (f) capacity retention plot for 4e.

NMC811, as clearly seen in the CV curve shown in **Figure 4a.** The lower first oxidation potential of ECF-NMC811 is due to the formation of a LiF surface layer that removes the surface carbonates/hydroxides and improves the ambient air stability. Apart from the initial non-equilibrium two-phase behavior, the first cycle oxidation peak in CV and initial voltage spike in the first charge is due to the ionically insulating coating that impedes the transport of Li ions out of the NMC811 phase.[7, 44] The ECF converts the insulating surface layer to ionically conducting/electronically insulating LiF, permitting the transport of Li-ion out/in of

the NMC phase and shutting down the parasitic interfacial reaction by blocking electron transport to the electrolyte side. Because of the robust CEI composed of LiF, the subsequent CV curves of ECF-NMC811 after the first cycle overlaps each other, indicating the stable interphase and reversibility of the lithium de/intercalation. In contrast, the CV curve of NMC811 does not overlap, indicating the unstable CEI. The current density for the CV plot of ECF-NMC811 is lower than the NMC811, also indicating that the LiF stabilized CEI controls the interfacial reaction. As a result of LiF stabilized interfaces, ECF-NMC811 exhibits improved cycling stability and enhanced capacity comparing to pristine NMC811, as shown in **Figure 4b**. The observation of the first high oxidation potential for NMC811 in the CV plot was supported by the first charge voltage plateau in **Figure S6**, and a similar trend was observed in the prior literature.[44]

Galvanostatic charge-discharge cycling experiments **(Figure 4b**) were performed at 0.1 C for the first two cycles for activation and then at 1C to investigate the effect of fluorination on cycling stability, rapid voltage fading, and capacity enhancement. Charge-discharge profiles at 1C are presented in **Figure 4c** and at 0.1C in **Figure S6**, respectively. Fluorination of NMC811 leads to enhanced stability and capacity (~4 % enhancement; initial charge discharge capacity of 219 mAh g^{-1} and 195 mAh g^{-1} for NMC811 compared to 236 mAh g^{-1} and 203 mAh g^{-1} for ECF-NMC811, respectively). Such a capacity enhancement for NMC811 with surface coating (alumina, ZrO_2, ZnO) and surface fluorination was also reported in the literature[8, 15], and this slight capacity enhancement for the ECF-NMC811 as compared with NMC811 may be due to the LiF stabilized surface of ECF-NMC811, which protects the interface and greatly reduces the formation of a basic surface film (LiOH, $Li2CO_3$) upon exposing to air during electrode fabrication and storage. As known from the literature, the formation of these residual lithium containing surface layers decreases the amount of extractable Li from the NMC811 cathode, thereby decreasing the specific capacity.[44] Besides, surface modification by LiF prevents the oxidation of transition metal octahedral network,

improves the crystallinity (seen in XRD, **Figure 1**), and controls the CEI thickness, resulting in higher capacity than pristine NMC811. As seen in **Figure 4b**, ECF-NMC811 exhibits better cycling stability with enhanced capacity than NMC811. At the end of 200 cycles, 13.7 % capacity fading was recorded for ECF-NMC811 as compared to ~22 % for NMC811. At 1 C rate, ECF-NMC811 delivers discharge capacity of 180.4 mAh g^{-1} with capacity retention of 86.3 % (after 200 cycles), 78 % (after 300 cycles), and 70.5 % (after 400 cycles) (**Figure 4d**). On the other hand, NMC811 delivers discharge capacity of 173.7 mAh g^{-1} with capacity retention of 78.0 % (after 200 cycles), 66.0 % (after 300 cycles), and 54.6 % (after 400 cycles). The cycling stability and capacity retention is even much better at a lower current rate. ECF-NMC811 delivers 203.4 mAh g^{-1} at a C/10 rate with capacity retention of 98.3 % after 100 cycles (**Figure 4e and 4f**) which is much higher compared ~85.0 % capacity retention of NMC811 after 100 cycles at the same condition (**Figure S7**). The improved electrochemical performance of ECF-NMC811 is because of the stabilized interfacial CEI layers via ECF engineered LiF on the electrode surface, confirmed by impedance spectroscopic analysis and surface analysis of electrode after cycling via XPS, (described later).

Effect of ECF in interfacial environments before and after cycling (2^{nd} at 0.1 C, 10^{th}, 25^{th}, 50^{th}, 75^{th}, 100^{th}, & 150^{th} at 1 C, 1C =200 $mAhg^{-1}$) was probed by electrochemical impedance spectroscopy (EIS). The impedance spectra are shown in **Figure 5 (a & b)** in which a semicircle from the high-to-intermediate frequency region corresponds to SEI impedance, charge-transfer resistance, and the slope at low frequency represents the diffusion of lithium ion in the bulk electrode material.[6, 45, 46] Before cycling, both ECF-NMC811 and NMC811 exhibit similar impedance which was mainly dominated by the resistive oxide layer present at lithium surface. During the cycling, total impedance of NMC811 decrease slowly and reaches to minimum at 25^{th} cycle (**Figure 5a**) which is similar to ECF-NMC811 at the 25^{th} cycles. However, the total impedance of ECF-NMC811 is much lower starting from the 2^{nd} cycle (**Figure 5b**), indicating the electrochemically stable CEI at ECF-NMC811 is interface-assisted

by LiF via ECF as compared to NMC811. From the 25th to 100th cycle, the impedance remains fairly stable with slight increments in both ECF-NMC811 and NMC811 interfaces. However, after 150th cycles, evolution of the impedance is much higher in NMC811 compared to ECF-NMC811 (**Figure S8**). This accurately correlates to the cycling data and explains the better capacity retention of ECF-NMC811 compared to NMC811. The lesser variation in EIS at the ECF-NMC811 interface indicates the formation of an electrochemically stable CEI assisted by LiF, that explains the benefit of having a LiF layer on the NMC811 surface & impacts on enhanced cycling stability and capacity retention.

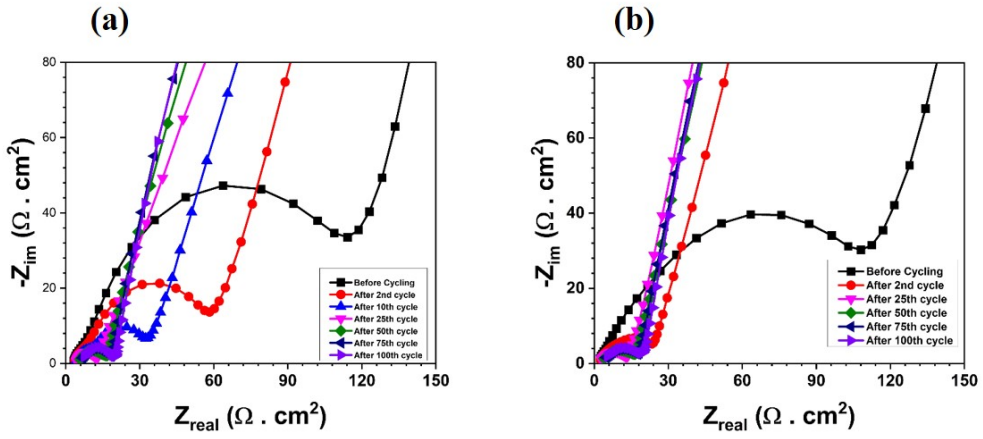

Figure 5. Evolution of impedance with increasing cycle number of (a) NMC811, and (b) ECF-NMC811.

To further investigate the significance of ECF modification on NMC811 on stabilizing the CEI, cycled cathode cells (after 100 cycles) were studied by XPS to identify the surface composition and determine the thickness of the CEI. The thickness results of the CEI and its composition on cycled NMC811 and ECF-NMC811 are shown in **Figure 6 (a-h) and Figure S9,** with wide energy survey spectrum shown in **Figure S10**. The C 1s spectrum (**Figure 6e**) of the cycled NMC811 electrode exhibits higher % C-F, C-C and C/O (C=O & C-O) and much more complex overlap between these species as compared to ECF-NMC811. A similar pattern was observed in O 1s spectra, in which both O-C and O=C bonded species were present (**Figure 6f**). F 1s spectra (**Figure 6g**) showed a similar amount of organic-F (C-F) species (binding

energy, B.E.~688 eV) for both NMC811 and ECF-NMC811 with much less inorganic-F (Li-F) species (B.E.~685 eV) in ECF-NMC811 as compared to NMC811. This was further corroborated by investigation of the depth profile (**Figure 6 (c & d)**), which shows much higher Li-F species present in NMC811. Li 1s spectra (**Figure 6h**) shows the existence of Li species (B.E.~56 eV) in CEI of both electrodes. **Figure S9** shows the P 2p spectra of cycled electrode which indicates much lower P species in the ECF-NMC811 interface than for NMC811; this was proven by Ar-ion etching that removes all P species (see **Figure 6 (b & d)**) after 15 sec sputtering time.

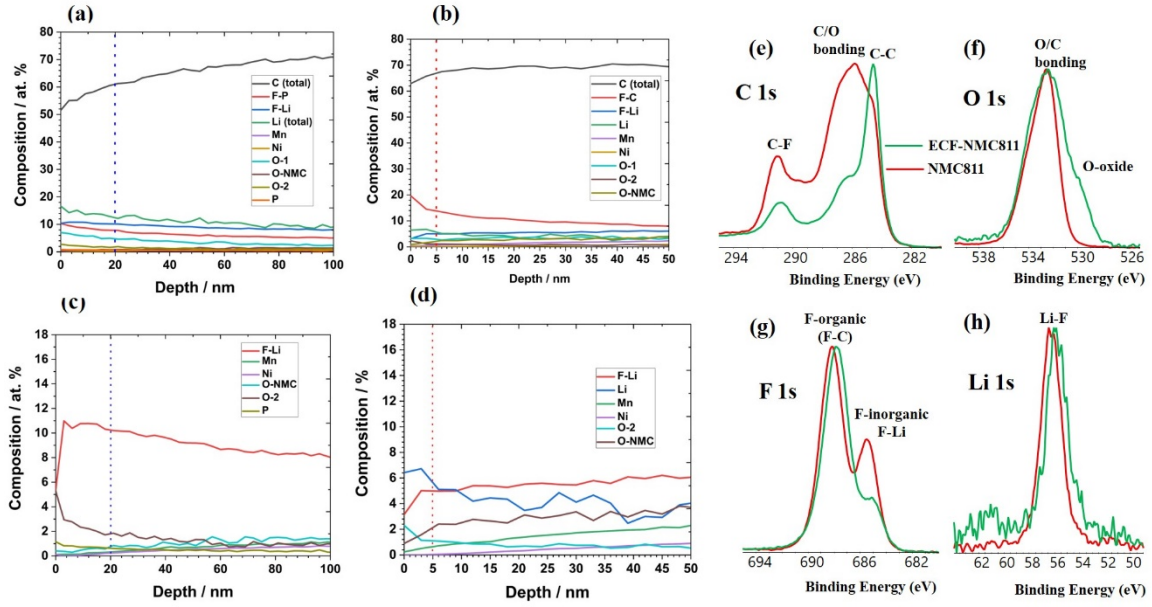

Figure 6. XPS depth profile measurements (a & c) for NMC811 showing CEI thickness > 20 nm marked by blue dotted line and (b & c) for ECF-NMC811 showing CEI thickness ~ 5 nm marked by red dotted line. Core level XPS spectra of (e) C 1s, (f) O 1s, (g) F 1s, & (h) Li 1s for NMC811 (red line) and ECF-NMC811 (green line)

The thickness of the CEI was determined by depth profiling via Ar-ion etching on cycled NMC811 and ECF-NMC811 electrodes. The carbon (C) profile shows that depth profile is removing an outer surface layer indicated by increasing C signal (**Figure 6 (a & b)**) - the data indicate a CEI thickness of > 20 nm in NMC811 and ~5 nm in ECF-NMC811. All of these facts - lower C-F, C/O, C-C, Li-F, & P species, and much thinner CEI at the ECF-NMC811

interfaces, suggest less electrolyte (carbonate solvents and $LiPF_6$) oxidation and side reactions occur at ECF-NMC811 interfaces than NMC811. This difference was made possible by the ECF induced LiF surface layer on the ECF-NMC811 electrode.

To investigate the structural changes and evolution of CEI after cycling, cathodes were imaged under HR-TEM after 100 charge/discharge cycles at 0.1 C rate. HR-TEM images (**Figure S11a**) of ECF-NMC811 after 100 cycles reveal the same lattice fringes as in pristine NMC811, with a d-spacing of ~0.47 nm along (003) plane that corresponds to layered oxide (NMC811) with R-3M space group; in addition, we have not observed any phase transition over the surface of the cathode. On the other hand, cycled NMC811 after 100 cycles has very thick non-uniform layer >19.0 nm on it's edge, (**Figure S11b & S11C**) which may be a combination of surface phase transition and products of uncontrolled parasitic interfacial reaction with electrolyte. This observation of surface phase transition and the formation of thick CEI on NMC811 is consistent with the literature[16], and this surface phase transition of NMC811 contributes to the rapid capacity fading of NMC811 described earlier. The HR-TEM data confirm that ECF results in very thin and uniform CEI compared to very thick non-uniform CEI on the NMC811 surface, as was suggested by impedance spectroscopic analysis and XPS analysis of the cycled electrode surface.

The effect of ECF-derived LiF surface layer on electrochemical performance was tested in full cells with ECF-NMC811 cathode and graphite anode, and compared with NMC811 cathode. **Figure S12 (a & b**) shows the charge-discharge profiles and coulombic efficiencies of these full cells from 3.0 – 4.2 V, collected at 0.1 C for two cycles and then at 0.5 C for 100 cycles. Though first cycle coulombic efficiency of NMC811 full cell (~84 %, charge capacity= 198.3 $mAhg^{-1}$, discharge capacity = 167.9 $mAhg^{-1}$) is slightly higher than ECF-NMC811 (81%, charge capacity= 211.4 $mAhg^{-1}$, discharge capacity = 171.3 $mAhg^{-1}$) (**Figure S12b**), the cycling stablity of ECF-NMC811 full cell (**Figure S12a**) is far better (capacity retention ~88 % for 100 cycles) than NMC811 (capacity retention ~35 % for 100 cycles), indicating the importance of

a continuous, protective LiF surface layer on the formation of stable CEI at the interface during cycling.

It has been demonstrated that the interlayer spacing and unit cell volume of NMC811 can collapse when the cell is cycled above 70 % SOC, resulting in sluggish lithium diffusion kinetics and making it harder to extract more lithium ions.[7] The overall cycling stability and capacity retention in ECF-NMC811 are much better than in NMC811, which may be because of robust CEI layer (thinner, better ionic conductor and electrical insulator) formed on ECF-NMC811 interface during charge/discharge assisted by thin LiF surface layer via ECF. Herein, we present the formation of the thin LiF surface layer on NMC811 surface via ECF (verified by XPS, STEM-EDX) that reduces the Ni/Li disordering as revealed by XRD analysis. Such a ionically conducting/electronically insulating thin LiF surface layer is beneficial for the stable electrochemical performance of the cathodes, which stabilizes the CEI as shown by electrochemical results and post analysis of the cathodes by EIS, XPS, HR-TEM analysis. These findings help reengineer the NMC811 interfaces to achieve the long cycling stability and capacity retention that will boost EV technology.

3. Conclusion

In conclusion, we have developed a promising ECF approach to enhance the electrochemical performance of battery cathode materials via a conformal LiF surface layer. The key features of ECF are better safety, significant cost reduction, easy industrial upscaling, and more promising delivery than existing tools. ECF was successfully deployed to fluorinate the surface of NMC811, which showed the effective tunability of the process for surface reengineering. ECF efficiently reduces the Ni/Li disordering, enhanced the layered structure stability, and lead to the formation of a robust very thin and uniform CEI composed of LiF layer on the surface of NMC811, all required for stable electrochemical performance. This results in enhanced capacity (~ 4 % capacity enhancement during the initial cycle) and improved stability

compared to pristine NMC811 (98 % capacity retention up to100 cycles at 0.1C rate, 86.4 % up to 200 cycles at 1 C rate for ECF-NMC811 compared to 78 % up to 200 cycles at 1 C rate for NMC811). As well as the LiF surface layer on ECF-NMC811 significantly enhanced the cycling stability of full cell with capacity retention of 90 % up to 100 cycles. These encouraging results proved that ECF could be an attractive tool to bolster the CEI on cathodes (NMC811 and other high-capacity high-voltage cathodes) that will enhance the cycling stability and capacity retention, critical criteria for electrification of daily transportation. Not only for the energy storage research, but this could also be extremely important for other material research fields such as photovoltaic solar cells, superconductors, electrocatalysts for OER, ORR, HER. A further and thorough study is necessary to explore the advantages of the ECF, which will open the new route for material functionalization for inorganic materials that will boost the energy density of energy storage devices via fluorinated electrodes.

4. Experimental Section

Materials and Methods: NMC811 was used as received. N-methyl imidazole (Alfa-Acer), bromoethane (Alfa-Acer), LiTFSI (3 M), polyethylene glycol (PEG200, Sigma-Aldrich), CsF (Sigma-Aldrich) were purchased and used as received.

Ionic liquids, Ethyl methyl imidazolium bis(trifluoromethanesulfonimide) (EMIM-TFSI), were prepared following an exactly similar procedure from the literature[47], using 1-methylimidazole instead of 1-methylpyrrolidine and bromoethane instead of 1-bromobutane. Electrolyte solution for the electrochemical fluorination was prepared by dissolving 0.5 M CsF in EMIM-TFSI with complexing agent PEG200 (0.5 M). PEG200 increases the solubility of CsF in EMIM-TFSI by complexing the Cs^+.

Electrochemical Fluorination (ECF): The experimental setup for ECF was shown in **Figure S13**. The ECF was carried out in ambient conditions in an undivided electrochemical cell. The electrochemical setup consists of a glass beaker, two electrodes (Ni mesh was used as anode

and cathode), a potentiostat, and an electrolytic solution (EMIM-TFSI with 0.5 M CsF with complexing agent PEG200). For the fluorination, metal oxide powders were pelletized using 2-ton pressures, and thus formed metal oxide pellets were wrapped by Ni mesh and used as a working electrode, and Ni mesh was also used as a counter electrode for fluorination. NMC811 pellets were fluorinated via anodic polarization (2.1 V) for 40 min at room temperature (See **Figure S14** for anodic fluorination profile) . The electrochemical charging profile for the anodic fluorination of NMC811 was shown in the supplementary information (**Figure S13**).

Materials Characterization: XRD pattern of the powder samples were collected on a Panalytical Empyrean diffractometer with Cu Kα radiation (0.154 nm) at 45 KeV and 40 mA over 2θ range from 10°- 90° angle. The surface composition was analyzed by acquiring XPS spectra with a Thermo Scientific (Waltham, MA, USA) model Kα instrument. The samples (powder and cycled electrodes) were loaded into the XPS vacuum transfer module from an Ar-filled glovebox and moved to the XPS load-lock and then introduced into the XPS analysis chamber with no air exposure. First, a wide energy range survey spectrum was acquired for each sample to determine all elements present followed by a set of narrow energy range core level spectra for each identified element. An Ar-ion etching depth profiling was performed cycled electrodes to quantify the thickness of CEI. The depth scale was computed using the sputtered time and rate with 12 nm/min. sputter rate on standard 100 nm films of SiO_2. HRTEM imaging was performed using a FEI Titan S/TEM operating at 300kV. Prior to imaging the samples were diluted in methanol and drop casted onto holey carbon grids and baked in vacuum for 8hrs at 160°C. Aberration correction STEM imaging was performed on JOEL NEOARM operating at 200 kV. The STEM-EDX data was collected on a FEI Talos 200X microscope operated at 200kV.

Electrochemical Characterization: Electrochemical performance of the NMC811 & ECF-NMC811 was evaluated in two-electrode coin cells (CR2032, Hohsen Corp. Japan, assembled in an Ar-filled glovebox) containing lithium metal as the reference/counter electrode, 1.2M LiPF6 in EC/DEC/DMC (ethylene carbonate/diethyl carbonate/dimethyl carbonate, 1:1:1 weight ratio) as the electrolyte, and Celgard 2320 as the separator (Celgard Inc., USA). The electrochemical performance of NMC811 & ECF-NMC811 was also evaluated in full-cell configuration using graphite anode in two-electrode coin cells. The working electrodes were prepared from slurries containing the active materials - pristine NMC811 and ECF-NMC811, conductive carbon (Super P Li), and PVDF (poly (vinylidene fluoride)) in a weight ratio of 80:10:10 dispersed in N-methyl pyrrolidone (NMP). After mixing homogeneously, the slurries were cast onto Al foil (pristine NMC811 and ECF-NMC811) using a doctor blade and dried at a vacuum oven at 100 °C for 24 hrs under high vacuum. Similar process was followed to cast the graphite electrode onto copper foil in weight ratio of 90:05:05. The working electrode disks (1/2" diameter) contained an active material loading of approximately 3.5 - 4 mg cm^{-2}. The galvanostatic charge-discharge cycling test for NMC811 electrodes was performed by polarizing the working electrode over 3.0 – 4.4 V vs. Li/Li^+ and 3.0 – 4.2 V vs graphite anode. Cyclic voltammetry (CV) of NMC811 electrodes was carried out between 3.0 – 4.3 V at a scan rate of 0.04 mV/s using a Bio-Logic VSP potentiostat.

Supporting Information

Supporting Information is available from the Wiley Online Library or from the author.

Notes

The authors declare no competing financial interest.

This manuscript has been authored by UT-Battelle, LLC, under contract number DE-AC05-00OR22725 with the US Department of Energy (DOE). The United States Government retains and the publisher, by accepting the article for publication, acknowledges that the United States

Acknowledgements

This work was supported by the U.S. Department of Energy, Office of Science, Office of Basic Energy Sciences, Materials Sciences and Engineering Division under contract number DE-AC05-00OR22725 with the US Department of Energy (DOE). The STEM-EDS analysis of this work used the Center for Functional Nanomaterials resources, a U.S. Department of Energy, Office of Science facility, Brookhaven National Laboratory under contact number DE-SC0012704. HRTEM imaging was conducted at the Center for Nanophase Materials Sciences, Oak Ridge National Laboratory which is a DOE Office of Science User Facility.

Received: ((will be filled in by the editorial staff))
Revised: ((will be filled in by the editorial staff))
Published online: ((will be filled in by the editorial staff))

References

[1] M. Armand, J. M. Tarascon, *Nature* **2008**, *451*, 652.

[2] D. Lin, Y. Liu, Y. Cui, *Nat. Nanotechnol.* **2017**, *12*, 194.

[3] M. S. Whittingham, *Chem. Rev.* **2004**, *104*, 4271-4302.

[4] J. M. Tarascon, M. Armand, *Nature* **2001**, *414*, 359-367.

[5] Y.-K. Sun, S.-T. Myung, B.-C. Park, J. Prakash, I. Belharouak, K. Amine, *Nat. Mater.* **2009**, *8*, 320.

[6] C. J. Jafta, X.-G. Sun, G. M. Veith, G. V. Jensen, S. M. Mahurin, M. P. Paranthaman, S. Dai, C. A. Bridges, *Energy Environ. Sci.* **2019**, *12*, 1866-1877.

[7] K. Märker, P. J. Reeves, C. Xu, K. J. Griffith, C. P. Grey, *Chem. Mater.* **2019**, *31*, 2545-2554.

[8] B. Song, W. Li, S.-M. Oh, A. Manthiram, *ACS Appl. Mater. Interfaces* **2017**, *9*, 9718-9725.

[9] A. Manthiram, B. Song, W. Li, *Energy Storage Materials* **2017**, *6*, 125-139.

[10] T. Weigel, F. Schipper, E. M. Erickson, F. A. Susai, B. Markovsky, D. Aurbach, *ACS Energy Lett.* **2019**, *4*, 508-516.

[11] F. A. Susai, D. Kovacheva, A. Chakraborty, T. Kravchuk, R. Ravikumar, M. Talianker, J. Grinblat, L. Burstein, Y. Kauffmann, D. T. Major, B. Markovsky, D. Aurbach, *ACS Appl. Energy Mater.* **2019**, *2*, 4521-4534.

[12] H.-H. Ryu, K.-J. Park, C. S. Yoon, Y.-K. Sun, *Chem. Mater.* **2018**, *30*, 1155-1163.

[13] W. Liu, P. Oh, X. Liu, M.-J. Lee, W. Cho, S. Chae, Y. Kim, J. Cho, *Angew. Chem. Int. Ed.* **2015**, *54*, 4440-4457.

[14] J. Kim, H. Lee, H. Cha, M. Yoon, M. Park, J. Cho, *Adv. Energy Mater.* **2018**, *8*, 1702028.

[15] U. Breddemann, E. M. Erickson, V. Davis, F. Schipper, M. Ellwanger, M. Daub, A. Hoffmann, C. Erk, B. Markovsky, D. Aurbach, I. Krossing, *ChemElectroChem* **2019**, *6*, 3337-3349.

[16] W. Xue, M. Huang, Y. Li, Y. G. Zhu, R. Gao, X. Xiao, W. Zhang, S. Li, G. Xu, Y. Yu, P. Li, J. Lopez, D. Yu, Y. Dong, W. Fan, Z. Shi, R. Xiong, C.-J. Sun, I. Hwang, W.-K. Lee, Y. Shao-Horn, J. A. Johnson, J. Li, *Nature Energy* **2021**, *6*, 495-505.

[17] X. Fan, X. Ji, L. Chen, J. Chen, T. Deng, F. Han, J. Yue, N. Piao, R. Wang, X. Zhou, X. Xiao, L. Chen, C. Wang, *Nature Energy* **2019**, *4*, 882-890.

[18] C. Niu, H. Pan, W. Xu, J. Xiao, J.-G. Zhang, L. Luo, C. Wang, D. Mei, J. Meng, X. Wang, Z. Liu, L. Mai, J. Liu, *Nat. Nanotechnol.* **2019**, *14*, 594-601.

[19] R. Tatara, Y. Yu, P. Karayaylali, A. K. Chan, Y. Zhang, R. Jung, F. Maglia, L. Giordano, Y. Shao-Horn, *ACS Appl. Mater. Interfaces* **2019**, *11*, 34973-34988.

[20] X. Fan, L. Chen, X. Ji, T. Deng, S. Hou, J. Chen, J. Zheng, F. Wang, J. Jiang, K. Xu, C. Wang, *Chem* **2018**, *4*, 174-185.

[21] X. Fan, L. Chen, O. Borodin, X. Ji, J. Chen, S. Hou, T. Deng, J. Zheng, C. Yang, S.-C. Liou, K. Amine, K. Xu, C. Wang, *Nat. Nanotechnol.* **2018**, *13*, 715-722.

[22] S. Chen, J. Zheng, D. Mei, K. S. Han, M. H. Engelhard, W. Zhao, W. Xu, J. Liu, J.-G. Zhang, *Adv. Mater.* **2018**, *30*, 1706102.

[23] F. Schipper, H. Bouzaglo, M. Dixit, E. M. Erickson, T. Weigel, M. Talianker, J. Grinblat, L. Burstein, M. Schmidt, J. Lampert, C. Erk, B. Markovsky, D. T. Major, D. Aurbach, *Adv. Energy Mater.* **2018**, *8*, 1701682.

[24] K. Meng, Z. Wang, H. Guo, X. Li, D. Wang, *Electrochim. Acta* **2016**, *211*, 822-831.

[25] W. Liu, X. Li, D. Xiong, Y. Hao, J. Li, H. Kou, B. Yan, D. Li, S. Lu, A. Koo, K. Adair, X. Sun, *Nano Energy* **2018**, *44*, 111-120.

[26] N. Pereira, F. Badway, M. Wartelsky, S. Gunn, G. G. Amatucci, *J. Electrochem. Soc.* **2009**, *156*, A407-A416.

[27] F. J. Brink, R. L. Withers, J. G. Thompson, *J. Solid State Chem.* **2000**, *155*, 359-365.

[28] H. Zhou, R. E. Ruther, J. Adcock, W. Zhou, S. Dai, J. Nanda, *ACS Nano* **2015**, *9*, 2530-2539.

[29] H. Zhou, J. Nanda, S. K. Martha, J. Adcock, J. C. Idrobo, L. Baggetto, G. M. Veith, S. Dai, S. Pannala, N. J. Dudney, *J. Phys. Chem. Lett.* **2013**, *4*, 3798-3805.

[30] B. P. Thapaliya, C. J. Jafta, H. Lyu, J. Xia, H. M. Meyer Iii, M. P. Paranthaman, X.-G. Sun, C. A. Bridges, S. Dai, *ChemSusChem* **2019**, *12*, 1316-1324.

[31] Z. Li, G. D. Del Cul, W. Yan, C. Liang, S. Dai, *J. Am. Chem. Soc.* **2004**, *126*, 12782-12783.

[32] P. F. Fulvio, S. S. Brown, J. Adcock, R. T. Mayes, B. Guo, X.-G. Sun, S. M. Mahurin, G. M. Veith, S. Dai, *Chem. Mater.* **2011**, *23*, 4420-4427.

[33] J. L. Adcock, P. F. Fulvio, S. Dai, *J. Mater. Chem. A* **2013**, *1*, 9327-9331.

[34] J. M. Powell, J. Adcock, S. Dai, G. M. Veith, C. A. Bridges, *RSC Adv.* **2015**, *5*, 88876-88885.

[35] B. P. Thapaliya, E. C. Self, C. J. Jafta, A. Y. Borisevich, H. M. Meyer Iii, C. A. Bridges, J. Nanda, S. Dai, *ChemSusChem* **2020**, *n/a*.

[36] R. A. House, L. Jin, U. Maitra, K. Tsuruta, J. W. Somerville, D. P. Förstermann, F. Massel, L. Duda, M. R. Roberts, P. G. Bruce, *Energy Environ. Sci.* **2018**, *11*, 926-932.

[37] X. Fan, E. Hu, X. Ji, Y. Zhu, F. Han, S. Hwang, J. Liu, S. Bak, Z. Ma, T. Gao, S.-C. Liou, J. Bai, X.-Q. Yang, Y. Mo, K. Xu, D. Su, C. Wang, *Nat. Commun.* **2018**, *9*, 2324.

[38] Y. P. Wu, E. Rahm, R. Holze, *Electrochim. Acta* **2002**, *47*, 3491-3507.

[39] K. Kang, G. Ceder, *Phys Rev B* **2006**, *74*, 094105.

[40] J. Zheng, Y. Ye, T. Liu, Y. Xiao, C. Wang, F. Wang, F. Pan, *Acc. Chem. Res.* **2019**, *52*, 2201-2209.

[41] T. Li, X.-Z. Yuan, L. Zhang, D. Song, K. Shi, C. Bock, *Electrochemical Energy Reviews* **2020**, *3*, 43-80.

[42] M. Wood, J. Li, R. E. Ruther, Z. Du, E. C. Self, H. M. Meyer, C. Daniel, I. Belharouak, D. L. Wood, *Energy Storage Materials* **2020**, *24*, 188-197.

[43] T. Fuchigami, S. Inagi, *Chem. Commun.* **2011**, *47*, 10211-10223.

[44] R. Jung, R. Morasch, P. Karayaylali, K. Phillips, F. Maglia, C. Stinner, Y. Shao-Horn, H. A. Gasteiger, *J. Electrochem. Soc.* **2018**, *165*, A132-A141.

[45] Y. Li, S. Wan, G. M. Veith, R. R. Unocic, M. P. Paranthaman, S. Dai, X.-G. Sun, *Adv. Energy Mater.* **2017**, *7*, 1601397.

[46] C. J. Jafta, X.-G. Sun, H. Lyu, H. Chen, B. P. Thapaliya, W. T. Heller, M. J. Cuneo, R. T. Mayes, M. P. Paranthaman, S. Dai, C. A. Bridges, *Adv. Funct. Mater.* **2021**, *31*, 2008708.

[47] B. Prasad Thapaliya, C.-L. Do-Thanh, C. J. Jafta, R. Tao, H. Lyu, A. Y. Borisevich, S. Yang, X.-G. Sun, S. Dai, *Batteries & Supercaps* **2019**, *0*.

The electrochemical fluorination (ECF) method is a robust fluorination method able to tune the surface functionalization forming conformal LiF, resulting in robust CEI and, in turn, results in enhanced electrochemical performance of a cathode. Cost-effective and free from all the hazards associated with state-of-the-art fluorination ensure its easy industrial upscaling.

Bishnu P. Thapaliya[*], *Sudhajit Misra, Shi-ze Yang, Charl J. Jafta, Harry M. Meyer III , Prashant Bagri, Raymond R. Unocic, Craig A. Bridges, Sheng Dai*[*]

Enhancing Cycling Stability and Capacity Retention of NMC811 Cathodes by Reengineering Interfaces via Electrochemical Fluorination